Journal of Structural Geology, Vol. 14, No. 10, pp. 1133 to 1148, 1992
Printed in Great Britain

0191-8141/92 $05.00+0.00

Physical explanation for the displacement–length relationship of faults using a post-yield fracture mechanics model

PATIENCE A. COWIE* and CHRISTOPHER H. SCHOLZ

Lamont-Doherty Geological Observatory and Department of Geological Sciences, Columbia University, Palisades, NY 10964-0190, U.S.A.

(*Received* 25 *June* 1991; *accepted in revised form* 27 *April* 1992)

Abstract—A plane strain model for a fault is presented that takes into account the inelastic deformation involved in fault growth. The model requires that the stresses at the tip of the fault never exceed the shear strength of the surrounding rock. This is achieved by taking into account a zone, around the perimeter of the fault surface, where the fault is not well developed, and in which sliding involves frictional work in excess of that required for sliding on the fully developed fault. The displacement profiles predicted by the fault model taper out gradually towards the tip of the fault and compare well with observed displacement profiles on faults. Using this model it is found that both (1) the shape of the displacement profile, and (2) the ratio of maximum displacement to fault length are a function of the shear strength of the rock in which the fault forms. For the case of a fault loaded by a constant remote stress, the displacement is linearly related to the length of the fault and the constant of proportionality depends on the shear strength of the surrounding rock normalized by its shear modulus. Using data from faults in different tectonic regions and rock types, the *in situ* strength of intact rock surrounding a fault is calculated to be on the order of 100 MPa (or a few kilobars). These estimates exceed, by perhaps a factor of 10, the strength of a well developed fault and thus provide an upper bound for the shear strength of the crust. It is also shown that the work required to propagate a fault scales with fault length. This result can explain the observation that the fracture energy calculated for earthquake ruptures and natural faults are several orders of magnitude greater than that for fractures in laboratory experiments.

INTRODUCTION

THIS paper is the first in a series of two papers on the subject of fault growth. Here we present a model that takes into account the physical processes by which new fault surface area is created at the ends of a fault. Using this model, we show that the ratio of maximum fault displacement to fault length is related to the shear strength of the surrounding rock. The second paper in this series (Cowie & Scholz 1992a) derives expressions, based on energetic and geometrical considerations, that relate seismic slip increments on a fault to the growth of the fault over geologic time.

Traditionally faults have been modelled as planar discontinuities or cracks in an otherwise elastic material. The reason for this modelling approach is that the material in which faults form, at least in the shallow crust, can support finite elastic strains. The elasticity of the Earth's crust is demonstrated by the occurrence of earthquakes and the flexural support of geologic loads. Various 'elastic' models have therefore been used to calculate stress and strain fields around a fault for specified conditions of displacement or stress on the fault surface (e.g. Chinnery 1961, Segall & Pollard 1980, Mavko 1982, Pollard & Segall 1987, Bilham & King 1989, King *et al.* 1989, Stein *et al.* 1989). However, in order to model fault growth one needs to relate the stresses at the tip of a fault to the fracture properties, in addition to the elastic properties, of the surrounding rock. A basis for understanding fault growth is provided by the theory of linear elastic fracture mechanics (LEFM), which relates the stresses at the tip of an idealized fault to the energy required for the fault to propagate. LEFM models have therefore been used to predict whether, and in which direction, a fault tip will propagate when subject to changes in the local stress field. Lin & Parmentier (1988) used LEFM to model the propagation of a normal fault as overburden pressure increases with depth in the crust. Aydin & Schultz (1990) used LEFM to predict whether the propagation of a strike-slip fault is enhanced or retarded in the vicinity of a neighboring fault segment. However, neither of these models specifically addressed the physical mechanism by which faults grow. Simple LEFM models, such as these, are limited in that it is assumed that the material around the fault tip is perfectly elastic. It is therefore implied that the inelastic processes (i.e. fracturing and frictional wear), involved in creating new fault surface area during growth, occur in a vanishingly small zone at the fault tip. Consequently, a simple LEFM model predicts that displacement on a fault should terminate abruptly with the maximum displacement gradient occurring right at the fault tip. This abrupt termination results in infinite stresses in the surrounding material in the vicinity of the fault tip, which is clearly unrealistic because real materials have finite strength.

Traditionally the inelastic zone at the tip of a fault has been ignored because of its structural complexity. This may be a valid approach if it can be demonstrated that the inelastic zone is small (e.g. Pollard and Segall 1987). However, by assuming that all the deformation is, to

*Present address: Laboratoire de Physique de la Matière Condensée, Université de Nice—Sophia Antipolis, CNRS URA 190, Parc Valrose, Nice 06000, France.

first order, elastic, only elastic material properties (e.g. shear modulus) appear in the equation that governs displacement on the fault. Consequently, there is no basis for understanding the physical mechanism of fault growth; in order to understand how a fault grows, it is necessary to specifically consider the zone of inelastic deformation at the fault tip.

Dugdale (1960) proposed a very simple model for inelastic deformation at the tip of a tensile crack in an elastic–plastic material. Goodier & Field (1963) (see also Bilby *et al.* 1963) subsequently obtained an expression for the crack displacement profile of the Dugdale model. The utility of the Dugdale model lies in the fact that the complexity of inelastic deformation is simply represented by a closing (or cohesive) stress that opposes the remote stress tending to open the crack. This closing stress corresponds to the stresses involved in plastically deforming the surrounding material. It is shown in this paper that Dugdale's approach can be used to develop a simple physical model for a fault that takes into account the inelastic deformation involved in fault formation and growth.

LABORATORY AND FIELD OBSERVATIONS

Until quite recently, observations detailed enough to evaluate an elastic crack model for faults were limited. Fault displacement data have mostly been gathered from field mapping of scarp heights and offset geologic markers; often only a few measurements have been taken on a single fault, most frequently the maximum displacement. Data on how displacement dies out towards the end of a fault, or on the structure of fault terminations, are invariably hard to obtain simply through lack of good exposure. Geodetic measurements are made at some distance away from a fault where the details of the fault tip make a small contribution to the regional strain field compared to the maximum amount of displacement in the center of the fault (Chinnery & Petrak 1967). Prior to the work of Rippon (1985), who mapped faults exposed in coal mines, very little was known about displacement on faults at depth, i.e. away from the effect of the free surface.

In the last 10 years or so, detailed information on faults and the mechanics of faulting has accumulated, for example: measurement of fault displacement profiles (e.g. Muraoka & Kamata 1983, Gudmundsson 1987a,b, Walsh & Watterson 1987, 1989, Opheim & Gudmundsson 1989, Peacock 1991, Peacock & Sanderson 1991, Villemin *et al.* in press) and fault termination strain fields (Hildebrand-Mittlefehldt 1979, 1980); studies of frictional wear on faults and the formation of gouge (e.g. Robertson 1982, Scholz 1987); laboratory and field studies of the growth of shear fractures and/or faults (e.g. Elliott 1976, Segall & Pollard 1983, Granier 1985, Etchecopar *et al.* 1986, Cox & Scholz 1988a,b, Martel *et al.* 1988).

Structural mapping indicates that faults are not single shear surfaces, but complex zones of brittle deformation (Aydin & Johnson 1978, Gay & Ortlepp 1979, Segall & Pollard 1983, Sibson 1986, Wallace & Morris 1986). Most well developed fault zones are surrounded by zones of pervasively fractured rock (Chester & Logan 1986). These fractures in many cases may be relics of the formation and growth of the fault: Cox & Scholz (1988a) used controlled laboratory experiments to show that Mode III shear cracks grow by generating and then coalescing arrays of tensile fractures ahead of the crack tip and that the shear surface eventually forms within a zone of fractured material. Figure 1 shows the progression of shear deformation, as demonstrated experimentally by Cox (1988) (Figs. 1a & b) compared to the structure of a natural fault mapped by Wallace & Morris (1986) (Fig. 1c). Knipe & White (1979) described a pattern of deformation, similar to that shown in Fig. 1, in shear zones in low-grade metamorphic terrains. Elliott (1976) observed what he termed a 'ductile bead', at the tips of propagating thrust faults: according to his description, "a non-cylindrical fold complex travels just ahead of a sideways propagating thrust. The rocks are folded, the folds grow and tighten, and then the thrust fracture extends laterally into this strained mass". Recent experimental work by Lockner *et al.* (1991) used acoustic emissions from a deforming rock sample to map the real time development of a shear fracture. From the pattern of acoustic sources, Lockner *et al.* (1991) showed that brittle deformation is initially distributed throughout the sample but as strain accumulates the deformation gradually localizes onto the ultimate failure plane.

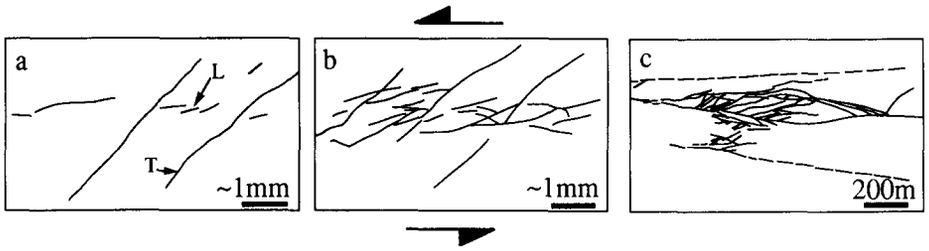

Fig. 1. Structural evolution of a shear fracture or fault. (a) Array of oblique tension (T) fractures represent the early stages of damage ahead of a propagating Mode III shear crack produced during a controlled rock fracture experiment (fracture is propagating out of the page towards the viewer); (b) subsequent development of the damage zone depicted in (a) marked by the intensification of fracturing and the formation of linking fractures (L). (a) & (b) modified from Cox (1988). Published with permission from S. J. D. Cox. (c) Cross-section through a fault zone in the Coeur d'Alene mine in Idaho mapped by Wallace & Morris (1986). Published with permission from Birkhaüser Verlag AG, Basel, Switzerland.

Each of the observations cited above involves the gradual accumulation and localization of inelastic deformation leading to the formation and growth of a fault or shear fracture. This is the process which we try to account for in the fault model developed in this paper. In detail, the deformation mechanisms are observed to be complex, as already discussed, involving both tensile fracturing and shearing of the surrounding rock (e.g. Fig. 1). Segall & Pollard (1983) and Martel *et al.* (1988) argue, based on field mapping of small fault zones in the Sierra Nevada granite, that faults in that area developed from pre-existing joints and did not grow in length by propagating as shear fractures through intact rock. The structural evolution of those fault zones involved the formation of tensile fractures which link the ends of en echelon joints, and the intensification of fracturing between closely spaced joints undergoing shear. In detail the observations of Segall & Pollard (1983) and Martel *et al.* (1988) differ from those described, for example, by Elliott (1976), but we consider their observations to be a particular case in a wide range of deformation mechanisms. For example, from field observations of similar small faults in granite in Massif de la Borne in France, Granier (1985) documented a much broader range of shear and tensile fracture mechanisms including some similar to those described by Segall & Pollard (1983).

The importance of inelastic deformation in faulting is also reflected in the shape of fault displacement profiles. Figure 2 shows stratigraphic separation diagrams for two normal faults. In each case displacement is greatest towards the center of the fault and decreases gradually towards the tips. A simple LEFM model for a fault in a perfectly elastic material would predict an elliptical displacement distribution in which the maximum displacement gradient occurs at the fault tip (e.g. see Pollard & Segall 1987), in contrast to the tapered or bell-shaped displacement profiles shown in Fig. 2. Our interpretation, supported by the results presented below, is that the tapering of the displacement profiles is a direct indication of inelastic deformation occurring in the volume surrounding the fault, particularly in the vicinity of the fault tip.

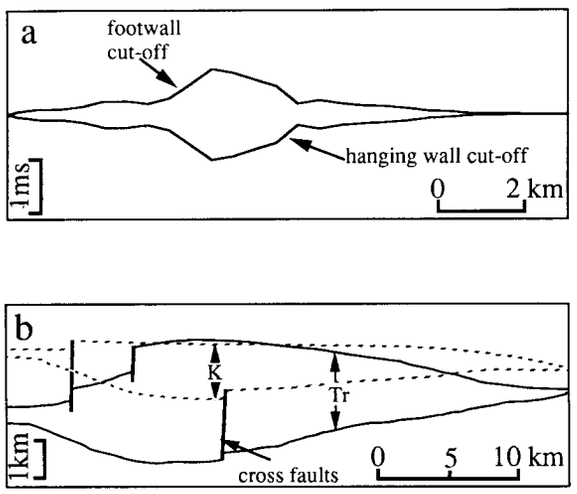

Fig. 2. Stratigraphic separation diagrams across normal faults: (a) a Plio-Quaternary normal fault in the Gulf of Corinth (modified from Higgs 1988). Published with permission from Blackwell Scientific Publications. Vertical scale in (a) is fault offset in two-way travel time. (b) The Saimo normal fault in the Kamasia Range of the Kenya Rift (modified from Chapman *et al.* 1978); K = separation of Cretaceous strata, Tr = separation of Triassic strata. Published with permission from the Geological Society of London. Vertical scale in (b) is fault offset in kilometers.

THE DUGDALE MODEL

The Dugdale model, and a similar model proposed by Barenblatt (1962), are referred to as cohesion zone models for a crack tip. Within the engineering literature, such models are the primitive end-member models within a specialist field called 'post-yield' or 'elastic–plastic' fracture mechanics (e.g. see Latzko *et al.* 1984, Kanninen & Popelar 1985). The model for faults presented here relies largely on qualitative and semi-quantitative observations. Therefore, we refer to the earliest papers on this subject where the basic principles are outlined and the parameters of the model can be related in the simplest way. Ida (1972), Palmer & Rice (1973) and Rice (1979, 1980), used this theory to develop the slip weakening model for earthquake rupture and a description of the energy fluxes through the crack tip region during propagation (see Rice 1968). Rudnicki (1980) and Li (1987) present comprehensive reviews of the applications of the slip weakening model to seismic rupture and creep events. Rubin (1990, 1991) considered the applications of cohesion zone models to the propagation of igneous dikes.

Dugdale (1960) considered a tensile (Mode I) crack cut in a material with an elastic–plastic rheology and loaded by a remote tensile stress (Fig. 3). As the tip of a crack produces a stress concentration, plastic deformation will initiate there if the stresses exceed the yield strength of the material, σ_y. The crack then extends a distance s, plastically deforming the region ahead of the tip. Yielding continues until the stress at the tip of the plastic zone just equals σ_y. Beyond the end of the inelastic zone the material still behaves elastically. It is assumed that plane strain conditions apply so that the displacement and stress fields around the crack are functions of x and y and that there is no deformation in the third dimension (Fig. 3a).

The Dugdale model is formulated by applying a uniform tensile (opening) stress, σ_r, over the total length of the crack, L, and a uniform closing stress, σ_y, acting over the length, s, at the ends of the crack (Fig. 3a). The stress intensity factor, which determines the magnitude of the stress field around the tip of a symmetrically loaded crack is given by (e.g. Lawn & Wilshaw 1975, equation 3.26):

$$K = 4\sqrt{\frac{L}{2\pi}}\int_0^{+L/2} \frac{\sigma(x)}{\sqrt{L^2 - 4x^2}}\,dx, \qquad (1)$$

where x is the distance measured from the center of the crack, and $\sigma(x)$ is the stress distribution on the crack faces. For the Dugdale model $\sigma(x) = \sigma_r$ over the range

$0 \leq x \leq L/2$, and $\sigma(x) = \sigma_y$ over the range $(L/2-s) \leq x \leq L/2$. An expression for the size of the inelastic zone, s is obtained by equating the stress intensity factor, K_o, due to σ_r alone with the stress intensity factor, K_i, due to σ_y alone. Setting K_o equal to K_i, s is then given by:

$$s = L \sin^2\left[\frac{\pi\sigma_r}{4\sigma_y}\right] \approx \frac{L\pi^2\sigma_r^2}{16\sigma_y^2}. \quad (2)$$

Note that L is the final yielded length of the crack (Fig. 3). For $s \leq 0.2L$ and $\sigma_y \geq 2\,\sigma_r$ the approximation, shown in (2), differs numerically from the full solution by $\leq$ 5%.

Equating the stress intensity factors enforces the requirement that the stress near the tip of the yielded crack is finite and moreover does not exceed σ_y. If the material is perfectly elastic, i.e. σ_y becomes infinite, then s in (2) approaches zero. Conversely, if σ_r is held constant, then as σ_y decreases s and thus L increase. The result expressed by (2) is illustrated in Figs. 3(b) & (c), where the crack opening displacement profile and the stress distribution in the plane of the crack are illustrated for two finite values of the yield strength, σ_y^1 and σ_y^2. As the yield strength decreases from σ_y^1 to σ_y^2, the length of the crack increases from L_1 to L_2 as the length of the yielded zones increases from s_1 to s_2. When σ_y becomes infinite the crack has an elliptical displacement distribution and there is a stress singularity at the crack tip (Fig. 3).

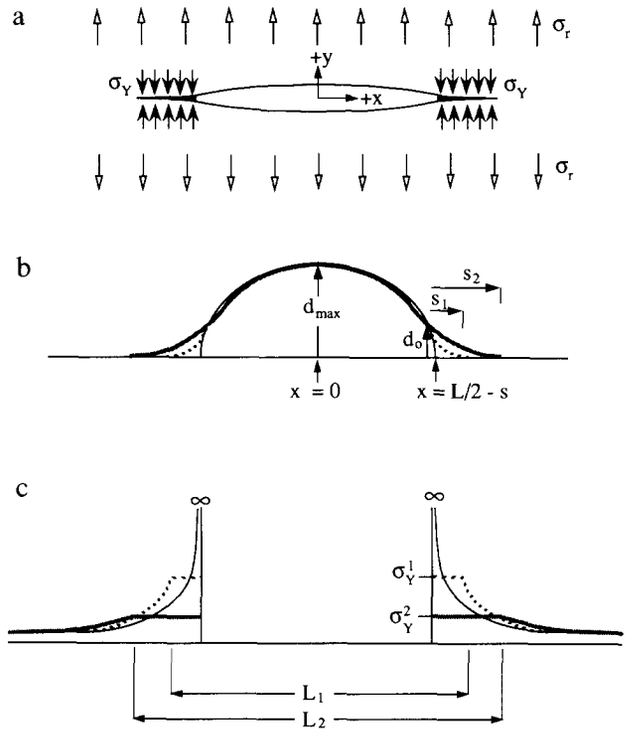

Fig. 3. (a) Dugdale model for a crack, of length L, loaded by a uniform remote tensile stress σ_r. Crack tip yielding extends the crack a distance s, doing work against a cohesive stress σ_y. The crack is parallel to the x-axis and is centered about $x = 0$. (b) Crack opening displacement profiles and (c) stress distribution for the model shown in (a). For finite values of the yield strength, σ_y the displacement profile is 'bell-shaped' with the maximum displacement, d_{max}, at the crack center, $x = 0$, and a displacement d_o at inflection points at $x = \pm((L/2) - s)$. The peak stress at the crack tips ($x = \pm L/2$) is equal to σ_y. As σ_y decreases from σ_y^1 to σ_y^2, s increases from s_1 to s_2, and the length of the crack increases from L_1 to L_2 (indicated by the dashed and shaded curves, respectively). In the limit $\sigma_y \to \infty$ the displacement profile becomes elliptical in shape and the stress at the crack tip becomes infinite (indicated by the thin solid lines).

Goodier & Field (1963) showed that for the geometry shown in Fig. 3(a), the displacement profile along the length of the crack is given by:

$$d(x) = \frac{(1-\nu)\,L\sigma_y}{2\pi\mu}\left[\cos\theta \log_e \frac{\sin^2(\theta_2 - \theta)}{\sin^2(\theta_2 + \theta)} + \cos\theta_2 \log_e \frac{(\sin\theta_2 + \sin\theta)^2}{(\sin\theta_2 - \sin\theta)^2}\right], \quad (3)$$

where ν is Poisson's ratio and μ is the elastic shear modulus. Note that (3) is the expression for the total displacement (in this case the total opening) on the crack, sometimes called the relative displacement (e.g. Pollard & Segall 1987). The trigonometric terms inside the bracket are the solutions to the elastic problem by the method of Muskhelishvili and are defined as:

$$\cos\theta = 2x/L \text{ for } |x| < L/2 \text{ and } \cos\theta_2 = (L - 2s)/L. \quad (4)$$

The maximum displacement at the center of the crack ($x = 0$) is given by:

$$d_{max} = \frac{(1-\nu)\,L\sigma_y}{2\pi\mu}\left[\cos\theta_2 \log_e \frac{(\sin\theta_2 + 1)^2}{(\sin\theta_2 - 1)^2}\right]. \quad (5)$$

In order to simplify (5) and to show the relationship between the ratio of maximum crack opening to crack length, d_{max}/L, and the material properties σ_y and μ, we may assume that the ratio $(L-2s)/L$ is a constant (i.e. the trigonometric terms in 5 are constant), in which case:

$$d_{max}/L \propto \sigma_y/\mu \quad (6)$$

and the ratio σ_r/σ_y is a constant. Alternatively, we may assume that $d_{max}/(L/2-s)$ is a constant but s is allowed to vary (illustrated in Fig. 3b), in which case:

$$\frac{d_{max}}{L} \propto \cos\left[\frac{\pi\sigma_r}{2\sigma_y}\right] \approx 1 - \frac{\pi^2\sigma_r^2}{8\sigma_y^2}. \quad (7)$$

In both (6) and (7), if μ increases, the ratio d_{max}/L decreases, which is what we expect from simple elastic crack theory, and as σ_y increases the ratio d_{max}/L increases.

By expanding the $\log_e$ terms in (3) as series and truncating after the first term, in the limit that σ_y tends to infinity so that θ_2 ends to zero, (3) reduces to:

$$d(x) = \frac{(1-\nu)\sigma_r}{\mu}\sqrt{L^2 - 4x^2} \quad (8)$$

which is the equation for the displacement distribution on a crack in a perfectly elastic material. Note that in this case the displacement on the crack depends only on μ and the remote stress σ_r, and no longer on the material yield strength σ_y.

The displacement profiles shown in Fig. 3(b) are 'bell-shaped' for finite values of σ_y. There is an inflection point in the displacement profile at the beginning of the

inelastic zone, $x = \pm(L/2 - s)$, and the magnitude of the displacement at this point, d_o, is given by (Goodier & Field 1963, equation A9):

$$d_o = \frac{2(1-\nu)\, L\sigma_y \cos\theta_2}{\pi\mu}[\log_e(\sec\theta_2)]. \quad (9)$$

Main points of the Dugdale model

The Dugdale model is a plane strain model for inelastic deformation at the tip of a Mode I crack. For the purposes of the following discussion the main points of the Dugdale model are summarized as follows:

(i) the displacement profile predicted by the model tapers out gradually towards the crack tip;

(ii) the peak stress at the tip of the crack just equals σ_y;

(iii) the material beyond the tip of the crack still deforms elastically;

(iv) the tapered shape is due to the presence of the inelastic zone at the tip of the crack;

(v) the size of the inelastic zone, s, decreases as the yield strength, σ_y, of the material containing the crack increases;

(vi) as σ_y approaches infinity (perfect elasticity) the Dugdale model becomes equivalent to a simple LEFM model; the crack opening displacement profile becomes elliptical in shape and the stress at the crack tip becomes infinite.

APPLYING THE DUGDALE MODEL TO FAULTS

The implications of using a model for a Mode I crack in a homogeneous material to describe Mode II or Mode III fault growth in a heterogeneous material like rock are clearly non-trivial. However, the reason we use this model is that it potentially provides a simple description of a complex process that is poorly understood, namely the role of inelastic deformation in fault development. Furthermore, the model invokes the requirement that for a crack at equilibrium under a system of applied stresses the peak stress at the crack tip cannot exceed the strength of the surrounding material. Equilibrium, or stable growth is a fundamental characteristic of fault propagation through the Earth's crust. We will show later that the basic characteristics of the Dugdale model, listed in the summary points (i)–(v) above, are also consistent with specific observations of faults.

Strictly speaking, the theoretical description of the Dugdale model pertains only to *large faults*, which are those that have lengths greater than the thickness of the brittle upper crust. Large faults grow by increasing their length (mapped trace length) while their down-dip width remains approximately constant, and are thus two-dimensional structures which may be modelled using a plane strain model. However, the conceptual framework for fault growth provided by the Dugdale model applies equally to small faults. We discuss the possible differences between small and large faults below.

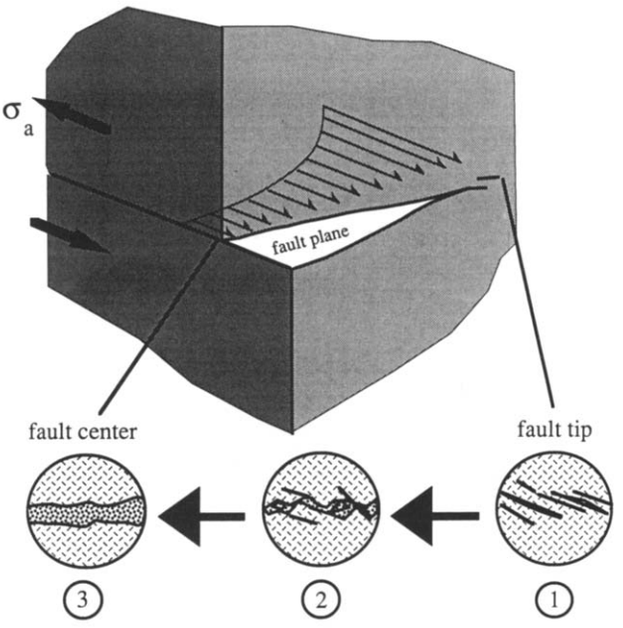

Fig. 4. Adaptation of the Dugdale model to a fault. Three stages are defined in the structural evolution of an idealized fault from the tip towards the center, approximately corresponding to the sequence depicted in Fig. 1. Stage (1): arrays of fractures; stage (2): coalescence of fractures to form an irregular immature fault; stage (3): well-developed fault achieved through continued mechanical wear as displacement accumulates. σ_a is the remote stress driving displacement on the fault indicated by the large left-lateral arrows. The frictional resistance on the fault is indicated by the thin arrows.

Following the formulation of the Dugdale model described above, it is assumed that the fault is loaded by a constant remote shear stress. The stress field across a deforming region will be maintained if the faults form and grow gradually and continuously (at least in a time averaged sense) in response to the imposed far field strain. The advantage of using a stress boundary condition is that the displacement on the fault can be related to frictional stresses on the fault surface and the shear strength of the material in which the fault forms.

In the Dugdale model for a crack in an elastic–plastic material, the yield strength corresponds to the stress at which the material no longer behaves elastically but starts to flow. For an elastic–brittle rheology it must correspond to the stress at which the material begins to fracture. However, rocks often contain many flaws ('Griffith Cracks') while still behaving in an overall elastic fashion. In the fault model we equate the material yield strength with the macroscopic shear strength, σ_o, of rock at ambient pressure and temperature conditions. At a microscopic scale the shear strength is due to fracturing across grains and sliding along intragrain contacts (e.g. Tapponier & Brace 1976), both of which are pressure dependent processes. Therefore, although the shear strength is primarily a function of lithology, it is not a constant material property but will be affected by confining pressure (e.g. Scholz 1990, fig. 1.12).

Here we argue that the cohesion zone in the Dugdale model corresponds to a zone near the fault tip where the fault surface is beginning to form but no through-going sliding surface is yet developed. Figure 4 shows a radial

cut across an idealized fault surface illustrating the change in structure of the fault from the tip towards the center, based on the evolutionary process depicted in Fig. 1. In stage 1 (Fig. 4), right at the fault tip, the surrounding rock is broken down by the formation of fractures. These fractures gradually coalesce to form an immature slip surface that is irregular and discontinuous. As the slip surface starts to accumulate displacement, the process of frictional wear smooths out the irregularities and an intermittent layer of fault gouge starts to form (stage 2, Fig. 4). Stage 3 in Fig. 4 represents the well developed fault surface which we assume characterizes an established through-going fault. These stages of development are similar to those described by Sibson (1988) based on observations from various published field studies.

The structural evolution shown in Fig. 4 is represented, in the fault model, by a varying shear resistance on a planar fault surface illustrated by the small arrows shown in the figure. The resistance to sliding on the fault surface is largest at the fault tip, where fractures first form and the fault is not well developed, but decreases as the displacement accumulates on the fault surface. Near the tip, the frictional resistance is a function of fracture development in rock, and as the displacement across the fault tends to zero, the frictional resistance must approach the shear strength, σ_o, of the surrounding rock. However, over the bulk of the established fault, the frictional properties are largely determined by the gouge layer that separates the sliding surfaces. Therefore, the well-developed fault is characterized by a residual frictional resistance, σ_f. During the initial stages of fault formation, mechanical erosion or wear of the fault surface is very high but as the fault continues to evolve with additional displacement it becomes a more continuous feature and can accommodate slip more easily. In the model, we call stages 1 and 2 in Fig. 4 the frictional breakdown zone of the fault (f.b.z. in Fig. 5). The frictional breakdown zone encompasses any distributed fracturing of the surrounding rock near the tip and the immature fault surface when the resistance to sliding exceeds, σ_f.

The relationship between frictional stress and displacement, described above, would imply a gradual decrease in the stress across the frictional breakdown zone of a fault. Ida (1972) considered a model in which σ_y (in the Dugdale model) varies in the inelastic zone and found that it is the value of σ_y that determines the magnitude of the stress concentration at the crack tip not the details of how it varies. Therefore, we approximate the increase in frictional resistance near the fault tip by a simple step (see Fig. 5).

Assuming that the accumulated displacement on a fault may be modelled as a freely-slipping crack with a residual frictional shear resistance, σ_f, the parameters σ_r and σ_y in equations (2)–(9), become $(\sigma_a - \sigma_f)$ and $(\sigma_o - \sigma_f)$, respectively. In this case, σ_a is the remotely applied shear tress loading the fault and σ_o is the shear strength of the surrounding intact rock. We adopt the convention that L is the length of the fault trace measured on a plane at, or parallel to, the Earth's surface (independent of whether it is a dip-slip or strike-slip fault). The length of the frictional breakdown zone, s, in this case is measured in the direction along the profile of a fault and corresponds to the region where the displacement tapers to zero with a convex-up shape (see Fig. 5). The displacement, d_o, is the offset across the fault at the beginning of the frictional breakdown zone ($x = L/2 - s$) and according to this model d_o coincides with an inflection point in the displacement profile (see Fig. 5).

Figure 6 shows four end-member solutions to equations (3) and (5) for different assumptions concerning $(\sigma_a - \sigma_f)$ and $(\sigma_o - \sigma_f)$, for a fault which accumulates displacement and increases in length over the time period from t_1 to t_2. This figure is arranged to show (from left to right) for each of the possibilities (Figs. 6a, d, g & j), the resulting relationship between maximum fault displacement and length (Figs. 6b, e, h & k) and the corresponding displacement profiles and stress distributions along the fault (Figs. 6c, f, i & l). In the first two cases (Figs. 6a & d) $(\sigma_a - \sigma_f)$ is not constant but decreases or increases as the fault grows. If $(\sigma_a - \sigma_f)$ decreases with time then the ratios s/L and d_{max}/L decrease as the fault grows (Figs. 6b & c). If $(\sigma_a - \sigma_f)$ increases with time then the ratios s/L and d_{max}/L increase as the fault grows (Figs. 6e & f), although this solution is no longer valid when $(\sigma_a - \sigma_f)$ exceeds $(\sigma_o - \sigma_f)$ because it implies that the rock fails catastrophically. Both of these solutions (Figs. 6a & d) fulfill the requirement that the maximum stress at the fault tip equals the rock shear strength, σ_o, for the actively growing fault. The solution obtained if $(\sigma_a - \sigma_f)$ is

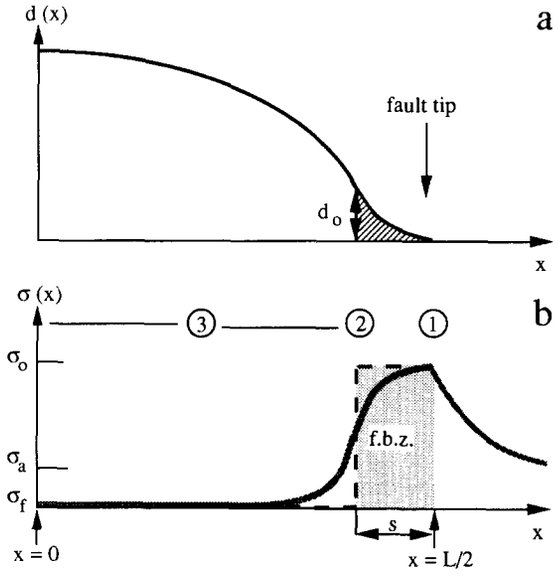

Fig. 5. (a) Displacement profile predicted by the model as a function of distance along the fault trace from the center ($x = 0$) out to the tip ($x = L/2$). (b) Variation of frictional resistance along the profile shown in (a) according to the structural evolution of the fault illustrated in Fig. 4. At the fault tip, where displacement is zero, frictional resistance approaches the shear strength of the surrounding rock, σ_o. Towards the center of the fault the frictional resistance equals the residual frictional value of the well-developed fault, σ_f. Numbered regions refer to stages indicated in Fig. 4, f.b.z. is the frictional breakdown zone of the fault of length, s, and d_o is the breakdown displacement which coincides with an inflection point on the displacement profile.

constant but $(\sigma_o - \sigma_f)$ increases, is shown in Fig. 6(g). In this case a linear relationship is obtained between d_{max} and L and the ratio s/L decreases through time (Figs. 6h & i). The solution shown in Fig. 6(j) corresponds to the case where both $(\sigma_a - \sigma_f)$ and $(\sigma_o - \sigma_f)$ are constant through time. For this solution the ratios d_{max}/L and s/L are constant, i.e. d_{max} and s increase linearly with the increase in L and lines of constant d_{max}/L ratio correspond to constant values of σ_o (Fig. 6k).

The solution shown in Figs. 6(j), (k) and (l) is the most physically reasonable solution for the general case. For example, consider a fault in which displacement accrues by a repetition of earthquakes. Slip on the fault is then governed by static and dynamic friction coefficients μ_s and μ_d on the well developed fault, so that $\sigma_a = \mu_s \sigma_n$ and $\sigma_f = \mu_d \sigma_n$, where σ_n is the effective normal stress on the fault. Then, when σ_n does not vary with fault length, $(\sigma_a - \sigma_f)$ varies only with $(\mu_s - \mu_d)$. Thus the cases shown in Figs. 6(a) & (d) imply that friction on the well developed portion of the fault continuously changes as the fault grows. This seems unreasonable, since after the initial breakdown friction should be scale independent (Scholz, 1990, pp. 91–92). The case shown in Fig. 6(g), on the other hand, assumes that $(\sigma_o - \sigma_f)$ increases as the fault grows. If anything, we expect that σ_o should decrease according to the size of the inelastic zone, i.e. $\sigma_o \propto 1/\sqrt{s}$ (see Scholz 1990, pp. 28–29), in which case we obtain the solution shown in Fig. 6(b) with S/L increasing, so this solution does not seem realistic either. Accordingly the case that is considered further in this paper is the case where $(\sigma_a - \sigma_f)$ and $(\sigma_o - \sigma_f)$ are constant during growth.

As a consequence of the lines of argument presented in the above fault model we also conclude that there is no *a priori* reason why small faults (those smaller than the thickness of the brittle crust) should exhibit a scaling relationship between fault displacement and length that is different from large faults. This is because the linear relationship depicted in Fig. 6(k) only depends on the far field stress and the shear strength of the rock in which the fault forms being approximately constant as the fault grows. While these conditions may depend in detail on the tectonic environment or, for example, variations in rock type, they do not depend on whether the fault is a

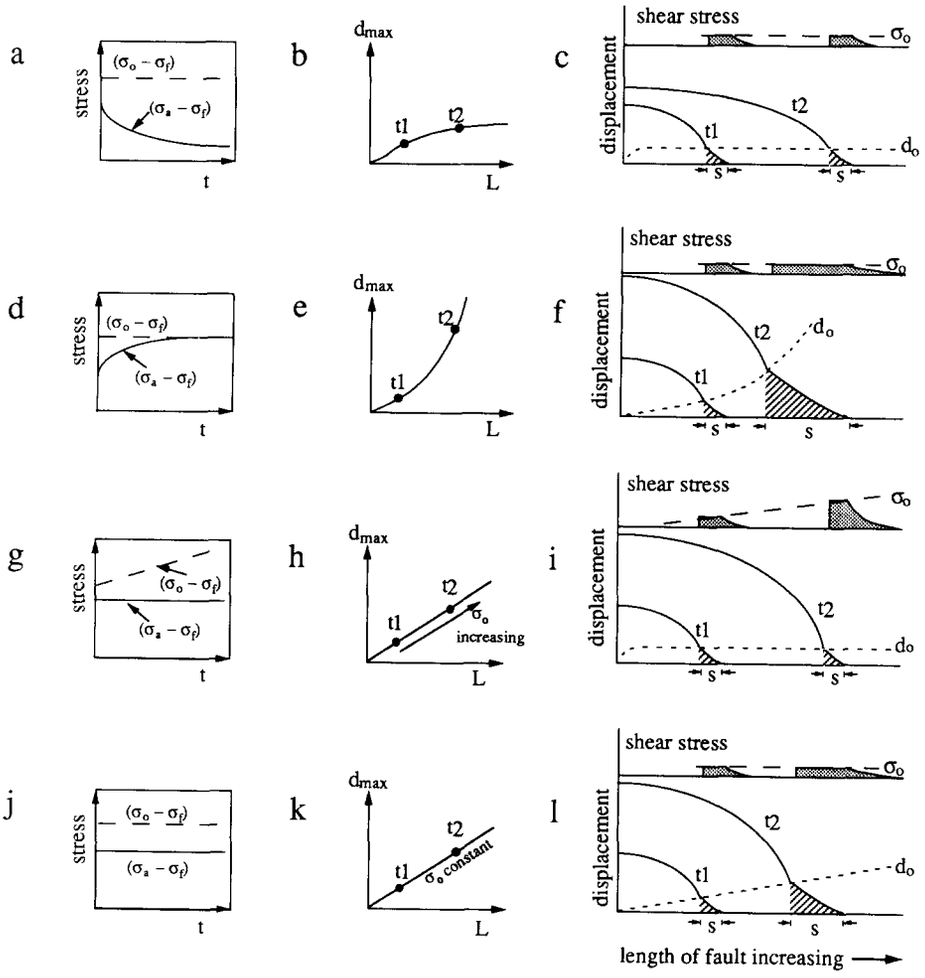

Fig. 6. Different possible solutions to the fault model (equations 3 and 5): (a), (d), (g) & (j) show how the boundary conditions $(\sigma_o - \sigma_f)$ and $(\sigma_a - \sigma_f)$ may vary through time; (b), (e), (h) & (k) show d_{max} as a function of fault length, L as the fault grows through time under the respective boundary conditions shown at left; (c), (f), (i) & (l) show the resulting fault displacement profiles in each case for times, t_1 and t_2, and the shear stress distribution in excess of σ_f is also indicated above in each case. Three end-member solutions are considered: (a), (b) & (c) refer to the case where $(\sigma_o - \sigma_f)$ remains constant and $(\sigma_a - \sigma_f)$ decreases with time; (d), (e) & (f) refer to the case where $(\sigma_o - \sigma_f)$ remains constant and $(\sigma_a - \sigma_f)$ increases; (g), (h) & (i) refer to the case in which $(\sigma_a - \sigma_f)$ is constant and $(\sigma_o - \sigma_f)$ increases; (j), (k) & (l) refer to the case in which both $(\sigma_o - \sigma_f)$ and $(\sigma_a - \sigma_f)$ remain constant. See text for discussion.

two-dimensional or a three-dimensional structure. However, it is probable that a constant geometrical factor in the scaling relationship will differ between small and large faults. For example, in simple elastic crack theory a circular crack in a volume (cf. small fault) has a ratio of maximum displacement to crack diameter that is 1.8 times larger than the ratio d_{max}/L of a two-dimensional crack in a plate (cf. large fault), all other variables remaining the same.

COMPARISON OF OBSERVATIONS WITH MODEL PREDICTIONS

The fault model described above relies on an oversimplification of inelastic deformation in rock around the fault tip. It assumes that the deformation is confined to a narrow zone extending in the plane of the fault and reflects the gradual mechanical breakdown of the surrounding rock to form a through-going fault. All the deformation involved in forming a through-going fault is represented in the model by an excess frictional resistance near the fault tip. The frictional breakdown zone of a fault is thus defined as a zone along the perimeter of the fault surface where the frictional resistance to sliding exceeds that on the well-developed central portion of the fault. As a consequence of using these assumptions, the model predicts several aspects of faulting that are consistent with observations.

Fault displacement profiles

The model predicts that the displacement on a fault decreases gradually towards the fault tip. Measured fault displacement profiles are characterized by finite displacement gradients at the tip and the gradients usually decrease towards the tip (e.g. Fig. 2). The fault displacement data shown in Fig. 7 are plotted as a function of distance from the center of the fault out to the tip, and the displacements and lengths are normalized to the largest value in each case, in order to show profiles for a range of fault sizes. For comparison, the displacement profile predicted by a simple LEFM model is also shown which plots as a circle on the normalized axes. Figure 7(a) shows seven displacement profiles collected by Muraoka & Kamata (1983) along normal faults exposed in lacustrine sediments in Japan. The measurements were made parallel to the slip vector, i.e. in the down-dip direction. In some cases lithologic variations in the sediments clearly modified the displacements recorded by Muraoka & Kamata (1983) so the data shown in Fig. 7(a) are restricted to those faults confined primarily to one lithology. The faults in this data set range in length from tens of centimeters to a few meters and have maximum displacements that are less than 10 cm. Figure 7(b) is taken from Walsh & Watterson (1987, their fig. 1) who compiled detailed measurements of displacement along normal faults in the Coal Measures in Britain. In this case the measurements were made along strike profiles, perpendicular to the slip vector and approximately parallel to the stratigraphy, so that the data are mostly obtained within the same lithology. The bold line in Fig. 7(b) is a composite displacement profile constructed from 34 individual profiles (see Walsh & Watterson 1987, their table 1). The faults in this data set range in length from several hundred meters to a few kilometers and have maximum displacements on the order of a few tens of meters. In both Figs. 7(a) & (b) the circular profile predicted by the elastic model overestimates the displacement at all points along the fault trace away from the maximum displacement. The profiles shown in Fig. 7(a) are approximately linear. The composite profile shown in Fig. 7(b) does exhibit a gradually increasing displacement gradient out to a distance of 0.5, a weak inflection at about 0.6, and then a decreasing displacement gradient towards the tip, as would be predicted by the Dugdale model (Figs. 3 and 5). Furthermore, the displacement profile shown in Fig. 7(b) implies that the inelastic zone, s, is a significant proportion of the total length of the fault, perhaps as much as 20%, i.e. the ratio s/L approximately equals 0.2. Also the displacement, d_o, measured at the infection point, is as much as 35% of the maximum fault displacement, i.e. the ratio d_o/d_{max} approximately equals 0.35.

Figure 8 shows displacement profiles from faults over a range of scales. The profiles are plotted from the center

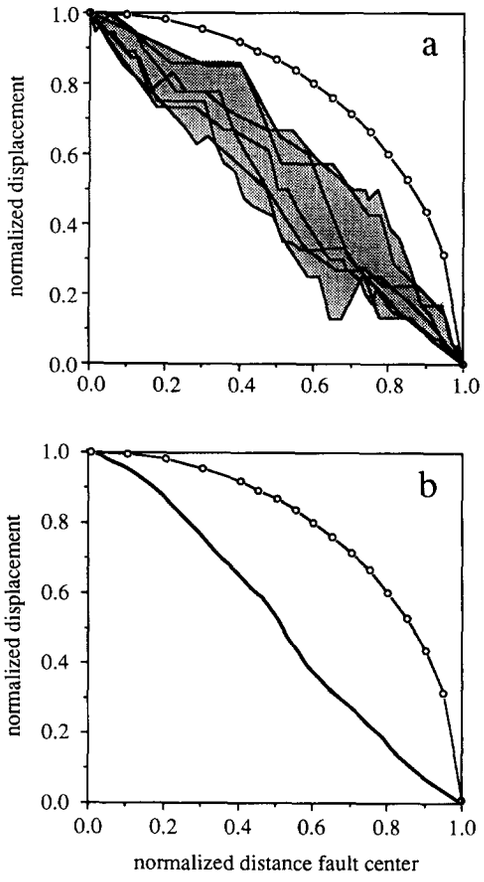

Fig. 7. Normalized fault displacement profiles (solid lines) compared to the elliptical profile predicted by a simple LEFM model (lines with dots). (a) Displacement profiles from seven faults in lacustrine sediments in Japan (data from Muraoka & Kamata 1983), shaded region shows the envelope that includes all the profiles; (b) Composite displacement profile constructed from 34 faults in the Coal Measures in Britain (taken from Walsh & Watterson 1987). See text for discussion.

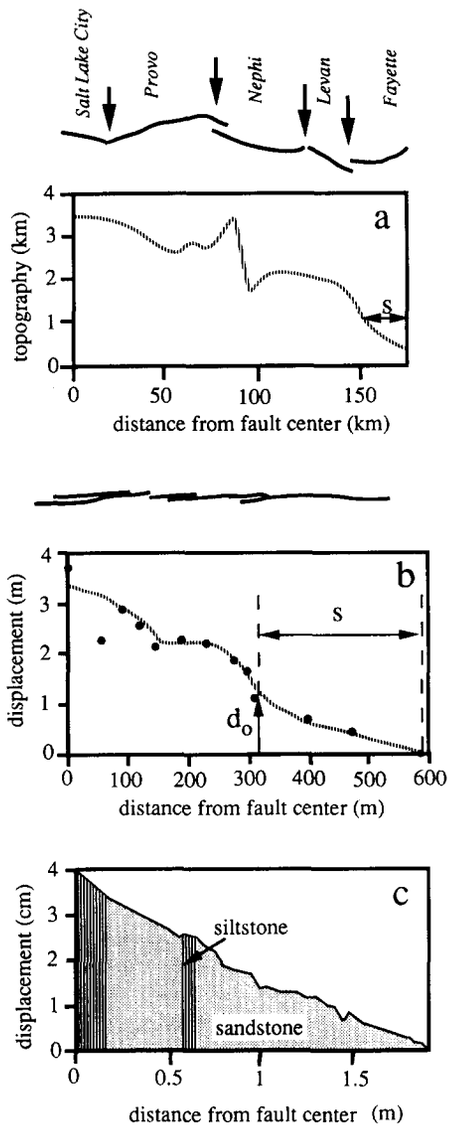

Fig. 8. Comparison of displacement profiles along faults at different scales. (a) Topographic profile along the footwall block of the Wasatch fault in Utah (from Schwartz & Coppersmith 1984—published with permission from the American Geophysical Union) with fault trace map above showing the named fault segments (from Machette *et al.* 1991). (b) Displacement profile along a normal fault in British coalfields (from Walsh & Watterson 1989) with fault trace is shown above. (c) Displacement profile from a normal fault in lacustrine sediments in Japan (from Muraoka & Kamata 1983). The parameters d_o and s, where they can be estimated, are also shown.

of the fault, where the displacement is greatest, out to the tip of the fault where the displacement dies to zero. Figure 8(a) is the topographic profile along the Wasatch Mountains which represent the uplifted footwall block along the Wasatch fault in the Basin and Range Province of the western United States. The Wasatch fault is approximately 360 km in total length (see Schwartz & Coppersmith 1984, Machette *et al.* 1991). The accumulated displacement along the fault zone is reflected by the height of the topography above the surrounding area which is approximately 3 km in the center of the fault. At the segment boundary between the Levan and Fayette segments there is an inflection point in the topographic profile separating the region of high elevations along the central part of the mountain range and the much lower elevations along the Fayette segment (see Fig. 8a). We suggest that the frictional breakdown zone of the macroscopic fault zone, indicated by s in Fig. 8(a), might be represented by the pattern of segmentation near the zone ends. In this case the ratio s/L approximately equals 0.14.

Figure 8(b) shows the fault trace and displacement data from a normal fault in the British coalfields published by Walsh & Watterson (1989). The distance from the center of the fault out to the fault tip is approximately 600 m and the maximum displacement on the fault is approximately 3.5 m. The displacement profile along the fault trace was obtained by summing the displacements on several strands. Walsh & Watterson (1989, 1991) demonstrate that together the separate strands behave as a single fault giving an overall tapered displacement profile. In this case, the shape of the displacement profile is quite similar to that predicted by the Dugdale model (Fig. 5). An inflection point in the profile occurs about 250 m from the fault tip and the displacement at this point is about 1.5 m. Therefore, according to our interpretation the ratio s/L approximately equals 0.2, and the ratio d_o/d_{max} approximately equals 0.4.

Figure 8(c) shows the displacement profile along a fault of only 1 m or so in length mapped by Muraoka & Kamata (1983). This fault, as well as other faults of similar size mapped by these workers and shown in Fig. 7(a), consists of a single strand. In contrast to the profiles shown in Figs. 8(a) & (b) the profile shown in Fig. 8(c) is approximately linear over its extent. These faults formed in poorly consolidated sediments. Therefore, one interpretation of these data is that the inelastic deformation is spread throughout the volume around the fault rather than localized at the fault tip. For example, linear crack opening displacement profiles are observed for tensile cracks in materials that exhibit large-scale plasticity (Kanninen & Popelar 1985).

The model presented here predicts that the stronger the rock in the vicinity of the tip, the more rapidly the displacement will die out towards the tip because the length of the breakdown zone, s, is inversely related to shear strength (e.g. see Fig. 3b). The discussions above assume the case of an isolated fault in a uniform applied stress field. In the case where two neighboring faults overlap, one may shield the other by locally reducing the applied stress, or alternatively may enhance the applied stress so that the effective strength of rock near the fault tip is increased. Muraoka & Kamata (1983), Walsh & Watterson (1989), Peacock (1991) and Peacock & Sanderson (1991) have found that the displacement gradient near the ends of fault segments is steeper if they overlap in this way.

Fault scaling relationships

The predictions of the model shown in Fig. 6 can be compared directly with fault displacement data. Measurements of the parameters d_{max}, L and estimates of d_o and s, have been obtained from an interpretation of displacement profiles along coalfield faults compiled by

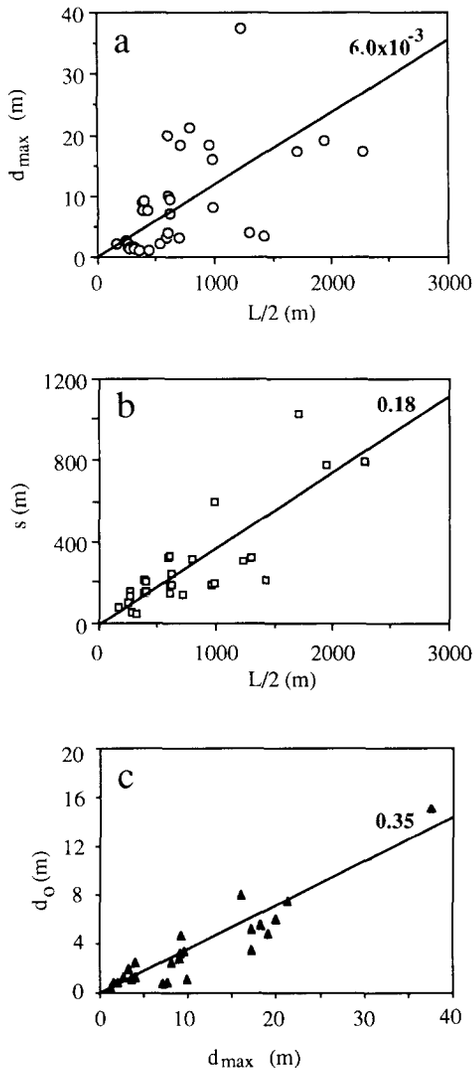

Fig. 9. Correlation between fault parameters using data from Coal Measure faults in Britain compiled by Walsh & Watterson (1987). Plots showing the variation of (a) d_{max} and (b) s as a function of fault radius $L/2$, and (c) d_o as a function of d_{max}. Solid lines indicate the approximate trend of the data in each case constrained to go through the origin and the estimates of the ratios d_{max}/L, s/L and d_o/d_{max} are shown in bold.

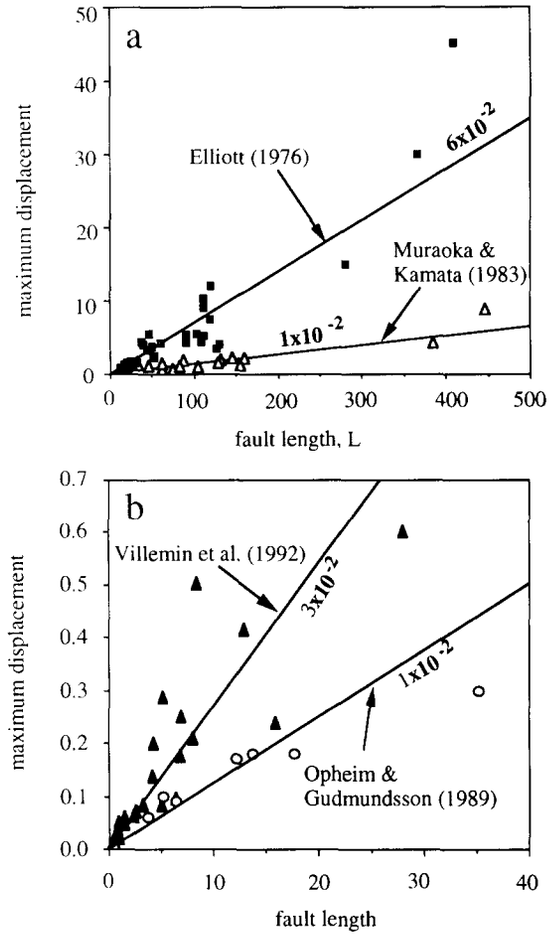

Fig. 10. Plots of d_{max} and L measured for faults in different tectonic regions and rock types. In order to compare data from very different length scales, the units on the axes vary between the data sets: Muraoka & Kamata (1983), normal faults in lacustrine sediments in Japan, lengths and displacements are both in centimeters; Elliott (1976), thrust faults in Canadian Rockies, lengths and displacements are both in kilometers; Opheim & Gudmundsson (1989), normal faults in Iceland, displacements and lengths are both in hundreds of meters; Villemin *et al.* (in press), normal faults in Lorraine Coalfield in France, lengths and displacements are both in kilometers. The estimated value of the ratio d_{max}/L is shown in bold in each case.

Walsh & Watterson (1987), and described above with reference to Fig. 7(b). In our interpretation, s is measured from the inflection point in a displacement profile out to the fault tip and d_o is the displacement at the inflection point (see Figs. 5 and 8, and discussion above). Figures 9(a) & (b) show the variation of d_{max} and s as a function of the half length or radius of the faults, $L/2$, each interpreted in the way shown in Fig. 8(b). For these coalfield faults s correlates linearly with L giving a constant ratio s/L of 0.18 (Fig. 9b). The data on d_{max} are more scattered but yield a value for the ratio d_{max}/L of approximately 6.0×10^{-3} (Fig. 9a). Figure 9(c) shows that the ratio d_o/d_{max} is approximately constant with a value of 0.35. The data shown in Fig. 9 are therefore most consistent with the solution shown in Figs. 6(j), (k) & (l) which predicts that the ratios d_o/d_{max}, s/L and d_{max}/L should be constant, i.e. these ratios should be independent of fault length.

An alternative interpretation of the variation of s or d_o with L shown in Fig. 9 is that these data may be reflecting different structural levels at which the displacement profiles were obtained. For example, s decreases if $(\sigma_o - \sigma_f)$ increases at greater depths (according the equation 2), so that two faults with different lengths sampled at different structural levels could yield the same s/L ratio, but if sampled at the same structural level may in fact yield different s/L ratios. However, it is hard to attribute the constant s/L ratio shown in Fig. 9(b) to a sampling effect, especially for an arbitrary sample of faults in a population.

Other available data sets, shown in Fig. 10, from faults in a variety of different tectonic regions and rock types have also been found to exhibit a linear relationship between d_{max} and L. Opheim & Gudmundsson (1989), in their study of normal faults in Iceland obtained a ratio d_{max}/L of about 1.2×10^{-2}. For normal faults in the Lorraine coalfield in NE France, Villemin *et al.* (in press) obtained 3.0×10^{-2}. Unpublished data of Elliott, from thrust faults in the Canadian Rockies (see Elliott 1976 for some of these data), gives a ratio of about

6.0×10^{-2}. Muraoka & Kamata (1983) estimated a value for this ratio of 1.2×10^{-2} for the meter-scale faults they mapped in Japan. The correlation between fault displacement and fault length has been variously interpreted by other workers (Watterson 1986, Walsh & Watterson 1988, Marrett & Allmendinger 1991). Elsewhere we provide a detailed discussion of the topic (Cowie & Scholz 1992b). However, we use these ratios below to estimate *in situ* values of rock shear strength for each data set, using the mathematical description of the fault model.

Deformation mechanisms near the fault tip

We have assumed in this model that the inelastic deformation is dominated by fracturing and frictional wear. Pressure solution and ductile flow may also be important deformation mechanisms particularly in sedimentary rocks such as limestone. Our interpretation of the linear displacement profiles shown in Figs. 7(a) and 8(c), discussed above, was that the soft sediments in which these faults form may exhibit large-scale plasticity rather than localized inelastic deformation at the fault tip. In contrast, from their observations of faulting in Coal Measure rocks, Walsh & Watterson (1987) described a monoclinal fold formed at the tips of laterally propagating normal faults and suggested this phenomena was analogous to the ductile bead of Elliott (1976) (see Introduction). In detail then, the deformation mechanisms occurring near the ends of a fault may be quite variable.

An illustration of the meaning of the breakdown zone of a natural fault is given in the map of a fault in the South Iceland seismic zone shown in Fig. 11. This fault was covered by several tens of meters of lava flows during Holocene times. In 1912, the fault ruptured in a strike-slip earthquake and propagated up into overlying, previously unfaulted, lava beds producing an en échelon array of tension fractures. The Iceland fault, as presently exposed at the surface, corresponds approximately to stage 1 of the fault model (Fig. 4). If the fault were to rupture again, the tension fractures now observed at the surface would begin to link up forming an irregular discontinuous fault trace. Only after several ruptures would a well developed fault eventually be formed (Cowie 1992, Chap. 3).

Fault tip strain field

According to the proposed fault model, the magnitude of the elastic stress or strain concentration beyond the end of the inelastic zone depends on the shape of the displacement distribution on the fault. Using a boundary element model, Chinnery & Petrak (1967) showed that a decreasing displacement gradient towards the fault tip, as predicted by the fault model, spreads the stress and strain concentration over a larger area. From detailed strain analyses, Hildebrand-Mittlefehldt (1979, 1980) found that the strain fields around the ends of an experimentally generated fault in clay and a naturally occurring normal fault were more consistent with Chinnery & Petrak's (1967) solution for a smoothly decaying displacement distribution than the solution for an abrupt termination in the displacement.

In the adaptation of the Dugdale model to faults, described above, the boundary of the frictional breakdown zone is related to a critical displacement d_0, on a planar fault surface. In nature, the frictional breakdown zone of a fault probably coincides with a transition from three-dimensional distributed deformation to displacement localized on a sliding surface. The boundary of the frictional breakdown zone occurs, in this case, where deformation near the fault tip eventually becomes localized to form a through-going fault. This critical amount of strain required to focus the deformation can be represented by the ratio d_0/s. For the Coal Measure faults discussed in relations to Figs. 7–9 this ratio is approximately 1.5×10^{-2}, which implies 1.5% strain.

ESTIMATES OF *IN SITU* ROCK PROPERTIES

Shear strength of rock

Using the fault model described in this paper, it has been shown that for a fault loaded by a constant remote stress, σ_a, and formed in rock with shear strength, σ_0, the maximum displacement on the fault is linearly related to its length. Modifying equation (5) to include the residual frictional stress on the fault, σ_f, the ratio d_{max}/L is given by:

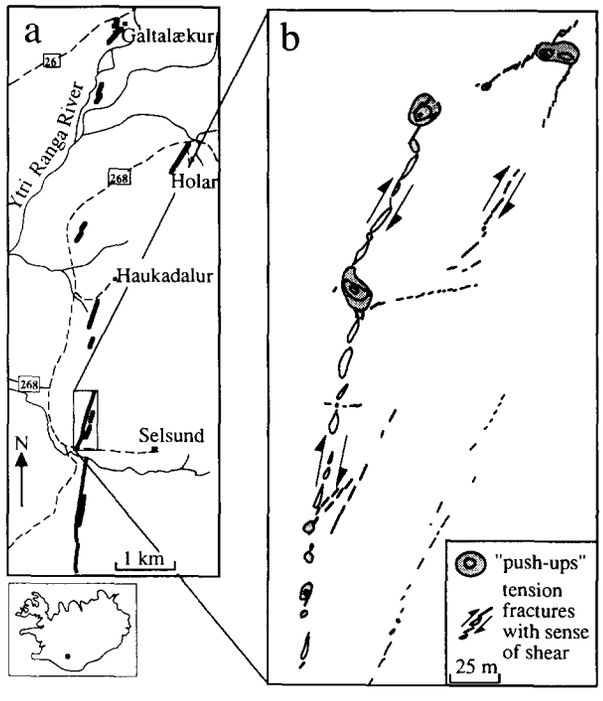

Fig. 11. Surface rupture of the 1912 earthquake in the South Iceland seismic zone. (a) Map showing the entire rupture zone, indicated by the heavy bold lines, where it is exposed in pahoehoe lava flows in southern Iceland. (b) Detailed map of a segment of the rupture showing the relationship between en échelon arrays of tension fractures and compressional 'push-ups' where the lava flow has been domed up between the ends of the fractures. Location shown in inset.

$$\frac{d_{max}}{L} = \frac{(1-\nu)(\sigma_o - \sigma_f)}{2\pi\mu}\left[\cos\theta_2 \log_e \frac{(\sin\theta_2 + 1)^2}{(\sin\theta_2 - 1)^2}\right]. \quad (10)$$

From equation (4), θ_2 equals $\cos^{-1}(1-2(s/L))$, where the ratio s/L is given by (from equation 2):

$$\frac{s}{L} \approx \frac{\pi^2(\sigma_a - \sigma_f)^2}{16(\sigma_o - \sigma_f)^2}. \quad (11)$$

Substituting the values for d_{max}/L (6.0×10^{-3}) and s/L (0.18) determined for the coalfield faults, and shown in Fig. 9, into (10) and (11) estimates of σ_o and σ_a can be obtained. The shear modulus of Coal Measure rocks, μ, is assumed to be 10 GPa (see Walsh & Watterson 1988). A lower value of σ_f is taken to be approximately 10 MPa from heat flow measurements, hydrofracture experiments and well bore breakouts in the vicinity of the San Andreas fault. An upper limit on σ_f of 50 MPa is calculated by assuming Coulomb friction with a friction coefficient of 0.75, a vertical stress equal to the lithostatic pressure under hydrostatic conditions, and by taking the maximum depth of formation of the faults to be 5 km. For σ_f equal to 50 MPa we find that σ_o is approximately 240 MPa (2.4 kbar) and σ_a is approximately 160 MPa (1.6 kbar), while if σ_f is only 10 MPa, σ_o is 200 MPa (2.0 kbar) and σ_a is 110 MPa (1.1 kbar). From these calculations it is found that $\sigma_a \approx \sigma_o/2$.

Using equation (9), we can calculate independent estimates of these same parameters, i.e.:

$$\frac{d_o}{L} = \frac{d_o}{d_{max}}\frac{d_{max}}{L} = \frac{2(1-\nu)(\sigma_o - \sigma_f)\cos\theta_2}{\pi\mu}[\log_e(\sec\theta_2)] \quad (12)$$

and $d_o/d_{max} = 0.35$. In this case, if σ_f is 50 MPa, σ_o is approximately 220 MPa (2.2 kbar) and σ_a is approximately 140 MPa (1.4 kbar), while if σ_f is only 10 MPa, σ_o is 180 MPa (1.8 kbar) and σ_a is 100 MPa (1.0 kbar).

According to (10) the observed range of the ratio d_{max}/L shown in Fig. 10 is reflecting changes in μ and σ_o of the rocks in which these faults formed as well as the ratio $(\sigma_a - \sigma_f)/(\sigma_o - \sigma_f)$. Both μ and σ_o depend on lithology; σ_a will depend on the tectonic environment. According to (10), if σ_a is constant, larger values of the ratio d_{max}/L imply larger values of σ_o, and if μ increases σ_o must also increase for a given d_{max}/L ratio.

Figure 12 shows the variation in the ratio d_{max}/L as a function of σ_o plotted for different values of μ and σ_f (using 10) Poisson's ratio ν was taken to be 0.2. Shear modulus, μ, varies with confining pressure particularly at low pressures because of the effect of crack closure and porosity reduction (e.g. Birch & Bancroft 1938, Brace 1964, Birch 1966). For example, in laboratory experiments μ typically increases by a factor of 1.5–2.0 up to pressures of 100 MPa. Assuming that confining pressure depends only on depth of burial then, for a crusty density of 2600 kg m^{-3}, confining pressure increases by approximately 26 MPa km^{-1}. At this rate laboratory values for μ would not be achieved shallower than approximately 4 km in the crust. This effect is likely to be greater in the crust because it contains much larger cracks than a laboratory sample. Furthermore, laboratory values are usually obtained from the shear wave velocity in a sample and these can exceed the static value of μ by 10–20% (e.g. Birch 1961, Judd 1964). In these calculations we use static values of μ, measured at pressures of ≤50 MPa, as follows: poorly compacted sedimentary rocks, μ = 3 GPa; crystalline rocks at shallow crustal depths and compacted sedimentary rocks, μ = 10 GPa; crystalline rocks at seismogenic depths, μ = 15 GPa. Finally, these values for μ are still likely to be overestimates of the shear modulus of the crust that would be effective at geologic strain rates.

In Fig. 12, we see that low displacement–length ratios for faults (i.e. 1.0×10^{-3}–5×10^{-3}) predict rock cohesive strengths in the range of 100–400 MPa (1–4 kbar) over the whole range of values of μ. Larger ratios of 5×10^{-2} may be achieved in rocks with relatively low shear rigidities (μ = 3 GPa) without requiring exceptionally large shear strengths (≤400 MPa). Ratios of 5.0×10^{-2} or greater in materials with a high shear modulus implies much larger shear strengths of 1.5–2 GPa (15–20 kbar), which are greatly in excess of laboratory estimates of shear strength at low confining pressures. Rock shear strength, σ_o, increases with increasing confining pressure and thus with depth in the crust. In experimental studies of rock fracture the strength of Westerly granite increases by approximately 5 MPa for an increase in confining pressure of 1 MPa (e.g. see Scholz 1990; fig. 1.12). Under ambient pressure and temperature conditions Westerly granite has a shear strength of 250 MPa. At a rate increase of confining pressure of 26 MPa km^{-1}, the strength of the bulk rock increases by 130 MPa km^{-1}. Therefore shear strengths on the order of GPa may be achieved at depths of ≥10 km in the crust where the confining pressure exceeds 200 MPa (2 kbar). Note that at these depths, ductile deformation may be more important than brittle deformation.

In order to interpret the variation in fault displacement–length ratios shown in Fig. 10 in terms of rock properties, the ratio s/L, determined from coalfield faults, is assumed to be the same for all the data sets.

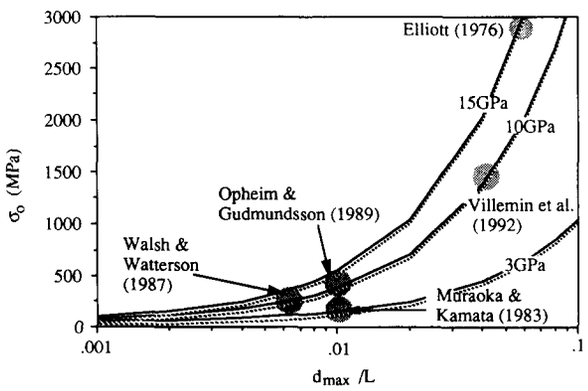

Fig. 12. Plot of rock shear strength σ_0 as function of the ratio d_{max}/L for different values of μ = 3, 10 and 15 GPa, using equation (10) with θ_2 = 0.88. Two curves are shown for each value of μ: dashed lines correspond to σ_f = 10 MPa; shaded lines correspond to σ_f = 50 MPa. Shaded circles indicate the location of the data sets shown in Figs. 9 and 10. Note that the horizontal axis is logarithmic.

Note that assuming a constant value for s/L is equivalent to assuming a constant value for the ratio $(\sigma_a - \sigma_f)/(\sigma_o - \sigma_f)$ (equation 11). This value for s/L is unlikely to be the same for faults from such different tectonic environments. However, the calculation is fairly insensitive to this parameter for $0.1 < s/L < 0.2$ which we believe to be a reasonable range of variation (see discussion above with reference to Figs. 7–9). Taking the range of values of d_{max}/L for each data set shown in Fig. 10 and assuming a probable value for μ in each case we have calculated a value for σ_o (Fig. 12). The large values of d_{max}/L for the faults in Elliott's unpublished data set and Villemin *et al.*'s (in press) data set are likely to be reflecting the fact that these faults penetrate to greater depths in the crust.

Any interpretation of these results is subject to the assumption that the mapped length of faults corresponds to the total length including the inelastic zone of the fault, s. As displacement towards the end of a fault is small and perhaps distributed over several fault strands there is a tendency to underestimate the length. As s apparently scales with L, L will always tend to be underestimated so that d_{max}/L and thus σ_o are overestimated. Furthermore, the model assumes that the observed displacement profile supports a corresponding elastic stress in the surrounding rock and does not allow for stress relaxation by bulk deformation during prolonged fault growth. If stress relaxation is an important effect, due to compaction, for example, in sedimentary rocks, then the measured displacement–length ratio will overestimate the *in situ* rock strength.

Fracture energy

In LEFM theory, the condition for crack propagation occurs when the stress intensity factor, K, at the crack tip reaches a critical value called the fracture toughness, K_c. The fracture energy, G, is proportional to $(K_c)^2$. In the fracture mechanics literature, the parameters, K_c and G are considered to be properties of the material and thus should be constant for a given rock type.

Estimates of G from experimental work and earthquakes do, however, show systematic variations that can not simply be attributed to differences in rock type (see Li 1987). Estimates of G from laboratory experiments of shear fracture development in intact samples are approximately 10^4 J m^{-2}. Martel & Pollard (1989) calculated similar values of G based on their field observations of slip on m–scale faults in granitic rocks. However, much smaller values of G (10–10^2 J m^{-2}) have been obtained from experiments using samples with an artificially introduced slip surface (e.g. Okubo & Dieterich 1984). In contrast, estimates of G from earthquakes are in the range $10^6 - 10^7$ J m^{-2}. The experimental work of Lockner *et al.* (1991) demonstrated that G varies, by perhaps a factor of two, depending on whether a shear crack is propagating under Mode II or Mode III conditions. Furthermore, shear fracture experiments show that G increases with increasing normal load (e.g. Cox & Scholz 1988a).

Li (1987) suggests that differences in G reflect the fact that the surface roughness of natural faults and fractures is much greater than that of artificially cut surfaces. Similarly, Martel & Pollard (1989) suggest that larger values of G determined from earthquakes on major fault zones, reflect the increased structural complexity of crustal-scale faulting compared to the outcrop-scale faults they mapped. Here we show that the range of estimates of G can be reconciled if each measurement is interpreted in terms of the critical crack length, L_c, at which an instability in crack growth occurs. In experimental studies, for example, L_c is the critical crack length formed in a sample when it fails (L_c is mm to cm). For earthquakes, L_c is the critical rupture dimension at which the rupture starts to propagate dynamically (L_c is 1–100 m).

For a cohesion zone crack model, such as that proposed for faults in this paper, Rice (1968) showed that the work done per unit length in propagating the crack, per unit width of the crack front, is given by:

$$G = \int_0^{d_o} [\sigma(d) - \sigma_f] \cdot \mathrm{d}d, \tag{13}$$

where $\sigma(d)$ is the variation in frictional resistance in the cohesion zone as a function of the displacement near the crack tip. The cohesion zone in this case is equivalent to the frictional breakdown zone, s, in the fault model, and d_o is the breakdown displacement. According to the model considered here $(\sigma(d) - \sigma_f)$ is a constant equal to $(\sigma_o - \sigma_f)$, so that integrating equation (13) we get:

$$G = (\sigma_o - \sigma_f) \cdot d_o. \tag{14}$$

Using the expression for d_o given in (9), (14) becomes:

$$G = \frac{2(1-\nu)\, L\, (\sigma_o - \sigma_f)^2 \cos\theta_2}{\pi\mu} [\log_e(\sec\theta_2)]. \tag{15}$$

Substituting into (15) the values of the various parameters determined for the coalfield faults above we find that $G \approx 5.0 \times 10^5\ L$ J m^{-2}, where L is measured in meters. Therefore, if L equals 1 mm–1 cm, G equals 5.0×10^2–5.0×10^3 J m^{-2} which agrees well with laboratory measurements. If $L = 100$ m, the upper estimate for earthquake ruptures, $G = 5.0 \times 10^7$ J m^{-2} according to this calculation. However, earthquakes rupture a pre-existing fault rather than intact rock so that it is more appropriate to use a stress difference $(\sigma_o - \sigma_f)$ comparable to earthquake stress drops, e.g. 10 MPa, in which case the calculated value for G is approximately 1.0×10^5 J m^{-2}.

Rice (1968) showed that if the size of the cohesion zone is sufficiently small so that frictional stresses on the crack faces can be ignored then G is just the elastic strain energy release rate (see Li 1987, equation 9.12). In general, G includes frictional dissipation. Whether friction is considered or not, the expression for energy release rate (i.e. fracture energy), of a crack of finite length in a material that deforms elastically (away from the immediate vicinity of the crack tip itself), includes

the term (stress)^2L (e.g. equation 15, and see Li 1987, equation 9.7). In this case, G is only a constant if both stress and crack length, L, are constant or stress varies systematically with L. The simplest interpretation, therefore, of the observed variation in G, is that the value of G corresponds to a critical crack or rupture dimension (i.e. $L = L_c$).

SUMMARY AND CONCLUSIONS

A post-yield fracture mechanics model, originally developed by Dugdale (1960) for Mode I cracks, is applied to the problem of accounting for the inelastic deformation involved in the formation and growth of a fault. The Dugdale model allows a simple physical model for a fault to be developed which does not require the details of the deformation at the fault tip to be specifically described. In this model, all inelastic deformation mechanisms are represented together by an increased frictional shear resistance around the perimeter of a planar fault surface. At the tip of the fault, where fractures are first formed but the fault is not well developed, the displacement is small and consequently the resistance to sliding is high; as the displacement tends to zero the frictional resistance approaches the shear strength of the surrounding rock. Towards the center of the fault, where the displacement is greater, the frictional resistance is decreased as the sliding surface develops due to mechanical breakdown of the rock.

The model is a plane strain or two-dimensional model and thus strictly speaking applies to large faults. However, the conceptual framework of this model applies equally to small faults. The model is parameterized by the maximum displacement on the fault, d_{max}, the breakdown displacement, d_o, and the mapped trace length of the fault, L, which includes the frictional breakdown zone of length s. In the model, the breakdown displacement, d_o, is achieved at the transition from an immature fault near the tip, to the well-developed central portion of the fault. The breakdown zone is the zone around the perimeter of the fault surface where the frictional resistance to sliding is in excess of that required to slip on the well developed central portion of the fault. For natural faults, the breakdown zone represents inelastic deformation near the fault tip which may be distributed in a volume; in this case, the ratio d_o/s can be thought of as the amount of shear strain at the tip of the fault necessary to focus distributed deformation into a through-going fault.

The model requires that the stress at the tip of a fault is finite and, moreover, can not exceed the shear strength of the surrounding rock. For an actively growing fault, rock at the fault tip is always at the point of failure while away from the fault, rock still deforms elastically. The specific deformation mechanism by which a fault fulfills the finite stress condition does not change the conclusions of the model. For example, this model does not require any assumptions to be made about how slip events on the fault are distributed to give the accumulated displacement profile, or whether fault linkage is a dominant growth mechanism. The model predicts the tapered shape of observed fault displacement profiles and provides expressions that relate the displacement distribution to the material properties of the surrounding rock.

Using this model we show that, for a fault loaded by a constant remote stress, the maximum displacement on a fault is linearly related to its length. The constant of proportionality depends on the ratio $(\sigma_o - \sigma_f)/\mu$, where σ_o is the shear strength of the surrounding rock, σ_f is the frictional resistance on the well-developed central portion of the fault and μ is the elastic shear modulus. Both σ_o and μ vary with lithology, while σ_o, μ and σ_f all vary strongly with confining pressure. Therefore this model predicts that faults in different tectonic regions and rock types will have a different ratio of displacement to length. This is consistent with available fault data sets. For a constant stress boundary condition, the size of the frictional breakdown zone and the breakdown displacement scale with the length of the fault. Consequently, we conclude that a fault maintains a self-similar displacement profile and structure through time.

Fault displacement–length data are used to estimate *in situ* values of the shear strength of rock. Using model parameters derived from an analysis of published data from British coalfield faults and assuming values for μ determined from laboratory measurements at temperatures and pressures representative of the crust, the following estimates of σ_o are obtained: weak sedimentary rocks, 100 MPa (μ = 3 GPa); indurated sedimentary rocks or fractured crystalline rocks, 100–500 MPa (μ = 10 GPa); crystalline rocks (at mid- to lower-crustal depths) 1–3 GPa (μ = 15 GPa). Values of σ_o obtained from fault data must be interpreted in terms of rock type in which the fault forms, the depth of formation, and variation in normal stress in the vicinity of the fault tip due to, for example, interaction with neighboring fault segments. The derived values of σ_o provide an upper estimate of *in situ* rock shear strength because the model does not allow for any relaxation of the stress field around the fault tip through time. However, according to these results the strength of the intact crust is much greater (by perhaps as much as 5–10 times) the frictional strength of through-going faults.

Finally, the expression for fracture energy derived for this model shows that if the breakdown displacement scales with fault length then fracture energy also scales with fault length. From the model we conclude that large variations in fracture energy measured from laboratory experiments, faults and earthquakes reflects large differences in the crack or rupture dimension at which an instability in growth occurs.

Acknowledgements—The authors wish to thank Jim Rice, Fred Chester, Geof King, Marc Spiegelman, John Walsh, Juan Watterson, Agust Gudmundsson, David Peacock, Alan Rubin and Chris Barton for useful discussions during the development of this work. Guy Reed and Bernie Coakley provided helpful comments on early versions of this manuscript. Jim Rice, Fred Chester, Steve Martel and Randy

Marrett provided very thorough and constructive reviews which considerably improved the final draft. This work was supported by NSF contract No. EAR90–04534. Lamont contribution number 4914.

REFERENCES

Aydin, A. & Schultz, R. A. 1990. Effect of mechanical interaction in the development of strike-slip faults with echelon patterns. *J. Struct. Geol.* **12**, 123–129.

Aydin, A. & Johnson, A. M. 1978. Development of faults as zones of deformation bands and as slip surfaces in sandstone. *Pure & Appl. Geophys.* **116**, 931–942.

Barenblatt, G. I. 1962. The mathematical theory of equilibrium cracks in brittle fracture. *Adv. Appl. Mech.* **7**, 55–125.

Bilby, B. A., Cottrell, A. H. & Swindon, K. H. 1963. The spread of plastic yield from a notch. *Proc. R. Soc. Lond.* **A272**, 304–314.

Bilham, R. & King, G. 1989. The morphology of strike-slip faults: examples from the San Andreas fault, California. *J. geophys. Res.* **94**, 10,204–10,216.

Birch, F. B. 1966. Compressibility; Elastic constants. In: *Handbook of Physical Constants. Mem. geol. Soc. Am.* **97**, 97–173.

Birch, F. B. 1961. The velocity of compressional waves in rock to 10 Kilobars, Part 2. *J. geophys. Res.* **66**, 2199–2224.

Birch, F. B. & Bancroft, D. 1938. The effect of pressure on the rigidity of rocks, 1. *J. Geol.* **46**, 59–87.

Brace, W. F. 1964. Brittle fracture of rocks. In: *State of Stress in the Earth's Crust* (edited by Judd, W. R.). Elsevier, New York, 111–178.

Chapman, G. R., Lippard, S. J. & Martyn, J. E. 1978. Stratigraphy and structure of the Kamasia range, Kenya Rift Valley. *J. geol. Soc. Lond.* **135**, 265–281.

Chester, F. M. & Logan, J. M. 1986. Implications for mechanical properties of brittle faults from observations of the Punchbowl fault zone, California. *Pure & Appl. Geophys.* **124**, 79–106.

Chinnery, M. A. 1961. The deformation of the ground around fault surfaces. *Bull. seism. Soc. Am.* **51**, 355–372.

Chinnery, M. A. & Petrak, J. A. 1967. The dislocation fault model with a variable discontinuity. *Tectonophysics* **5**, 513–529.

Cowie, P. A. 1992. The growth of faults. Unpublished Ph.D. thesis, Columbia University, New York.

Cowie, P. A. & Scholz, C. H. 1992a. Growth of faults by accumulation of seismic slip. *J. geophys. Res.* **97**, 11,085–11,096.

Cowie, P. A. & Scholz, C. H. 1992b. Displacement–length scaling relationship for faults: data synthesis and discussion. *J. Struct. Geol.* **14**, 1149–1156.

Cox, S. J. D. 1988. *Experimental study of the growth of shear cracks.* Unpublished Ph.D. thesis, Columbia University, New York.

Cox, S. J. D. & Scholz, C. H. 1988a. Rupture initiation in shear fracture of rocks: An experimental study. *J. geophys. Res.* **93**, 3307–3320.

Cox, S. J. D. & Scholz, C. H. 1988b. On the formation and growth of faults. *J. Struct. Geol.* **10**, 413–430.

Dugdale, D. S. 1960. Yielding of steel sheets containing slits. *J. Mech. Phys. Solids* **8**, 100–104.

Elliott, D. 1976. The energy balance and deformation mechanisms of thrust sheets. *Phil. Trans. R. Soc. Lond.* **A283**, 289–312.

Etchecopar, A., Granier, T. & Larroque, J.-M. 1986. Origine des fentes en echelon: propagation des failles. *C.r. Acad. Sci., Paris* **302**, 479–484.

Gay, N. C. & Ortlepp, W. D. 1979. Anatomy of a mining induced fault zone. *Bull. geol. Soc. Am.* **90**, 47–58.

Goodier, J. N. & Field, F. A. 1963. Plastic energy dissipation in crack propagation. In: *Fracture of Solids* (edited by Drucker, D. C. & Gilman, J. J.). Wiley, New York, 103–118.

Granier, T. 1985. Origin, damping and pattern of development of faults in granite. *Tectonics* **4**, 721–737.

Gudmundsson, A. 1987a. Geometry, formation and development of tectonic fractures on the Reykjanes Peninsular, southwest Iceland. *Tectonophysics* **139**, 295–308.

Gudmundsson, A. 1987b. Tectonics of the Thingvellir fissure swarm, SW Iceland. *J. Struct. Geol.* **9**, 61–69.

Higgs, W. 1988. Syn-sedimentary structural controls on basin deformation in the Gulf of Corinth, Greece. *Basin Res.* **1**, 155–165.

Hildebrand-Mittlefehldt, N. 1979. Deformation near a fault termination, Part I: A fault in a clay experiment. *Tectonophysics* **57**, 131–150.

Hildebrand-Mittlefehldt, N. 1980. Deformation near a fault termination, Part II: A normal fault in shales. *Tectonophysics* **64**, 211–234.

Ida, Y. 1972. Cohesive force across the tip of a longitudinal-shear crack and Griffith's specific surface energy. *J. geophys. Res.* **77**, 3796–3805.

Judd, W. R. 1964. Rock stress, rock mechanics, and research. In: *State of Stress in the Earth's Crust* (edited by Judd, W. R.). Elsevier, New York, 5–53.

Kanninen, M. F. & Popelar, C. H. 1985. *Advanced Fracture Mechanics.* Oxford University Press, Oxford.

King, G. C. P., Stein, R. S. & Rundle, J. B. 1989. The growth of geologic structures by repeated earthquakes, 1, Conceptual framework. *J. geophys. Res.* **93**, 13,307–13,318.

Knipe, R. J. & White, S. H. 1979. Deformation in low grade shear zones in the Old Red Sandstone, southwest Wales. *J. Struct. Geol.* **1**, 53–66.

Lawn, B. R. & Wilshaw, T. R. 1975. *Fracture of Brittle Solids.* Cambridge University Press, Cambridge.

Latzko, D. G. H., Turner, C. E., Landes, J. D., McCabe, D. E. & Hellen, T. K. 1984. *Post-yield Fracture Mechanics.* Elsevier, New York.

Lockner, D. A., Byerlee, J. D., Kuksenko, V., Ponomarev, A. & Sidorin, A. 1991. Quasi-static fault growth and shear fracture energy in granite. *Nature* **350**, 39–42.

Li, V. C. 1987. Mechanics of shear rupture applied to earthquake zones. In: *Fracture Mechanics of Rock* (edited by Atkinson, B.). Academic Press, London.

Lin, H. & Parmentier, M. 1988. Quasi-static propagation of a normal fault: a fracture mechanics model. *J. Struct. Geol.* **10**, 249–262.

Machette, M. N., Personius, S. F., Nelson, A. R., Schwartz, D. P. & Lund, W. R. 1991. The Wasatch fault zone, Utah — segmentation and history of Holocene earthquakes. *J. Struct. Geol.* **13**, 137–149.

Marrett, R. & Allmendinger, R. W. 1991. Estimates of strain due to brittle faulting: sampling of fault populations. *J. Struct. Geol.* **13**, 735–737.

Martel, S. J., Pollard, D. D. & Segall, P. 1988. Development of simple strike-slip fault zones, Mount Abbot Quadrangle, Sierra Nevada, California. *Bull. geol. Soc. Am.* **100**, 1451–1465.

Martel, S. J. & Pollard, D. D. 1989. Mechanics of slip and fracture along small faults and simple strike-slip fault zones in granitic rock. *J. geophys. Res.* **94**, 9417–9428.

Mavko, G. M. 1982. Fault interaction near Hollister, California. *J. geophys. Res.* **87**, 7807–7816.

Muraoka, H. & Kamata, H. 1983. Displacement distribution along minor fault traces. *J. Struct. Geol.* **5**, 483–495.

Okubo, P. G. & Dieterich, J. H. 1984. Effects of fault properties on frictional instabilities produced on simulated faults. *J. geophys. Res.* **89**, 5817–5827.

Opheim, J. A. & Gudmundsson, A. 1989. Formation and geometry of fractures, and related volcanism, of the Krafla fissure swarm, northeast Iceland. *Bull. geol. Soc. Am.* **101**, 1608–1622.

Palmer, A. C. & Rice, J. R. 1973. The growth of slip surfaces in the progressive failure of overconsolidated clay. *Proc. R. Soc. Lond.* **A332**, 527–548.

Peacock, D. C. P. & Sanderson, D. J. 1991. Displacement, segment linkage and relay ramps in normal fault zones. *J. Struct. Geol.* **13**, 721–733.

Peacock, D. C. P. 1991. Displacement and segment linkage in strike-slip fault zones. *J. Struct. Geol.* **13**, 1025–1035.

Pollard, D. D. & Segall, P. 1987. Theoretical displacements and stresses near fractures in rock: with applications to faults, joints, veins, dikes and solution surfaces. In: *Fracture Mechanics of Rock* (edited by Atkinson, B.). Academic Press, London.

Rice, J. R. 1968. In: *Fracture: An Advanced Treatise, Volume 2* (edited by Leibowitz, H.), Academic Press, New York, 191–331.

Rice, J. R. 1979. Theory of precursory processes in the inception of earthquake rupture. *Gerlands Beitr. Geophys.* **88**, 91–127.

Rice, J. R. 1980. The mechanics of earthquake rupture. In: *Physics of the Earth's Interior, Proc. Int. Sch. Phys. Enrico Fermi* (edited by Dziewonski A. & Boschi E.). North-Holland, Amsterdam, 555–649.

Rippon, J. H. 1985. Contoured patterns of the throw and hade of normal faults in the Coal Measures (Westphalian) of northwest Derbyshire. *Proc. Yorks. geol. Soc.* **45**, 147–161.

Robertson, E. C. 1982. Continuous formation of gouge and breccia during fault displacement. In: *Issues in Rock Mechanics, Proc. 23rd Symp. Rock. Mech.* (edited by Goodman, R. E. & Hulse, F.). Am. Inst. Min. Engrs., New York, 397–404.

Rubin, A. M. 1990. Rock fracture at high confining pressure and the scale dependance of the damage zone at the tips of propagating dikes. *Trans. Am. Geophys. Un.* **71**, 635.

Rubin, A. M. 1991. Rock fracture during dike propagation: Reconciling field observations with laboratory experiments. *Trans. Am. Geophys. Union* **72**, 442.

Rudnicki, J. W. 1980. Fracture mechanics applied to the Earth's crust. *Annu. Rev. Earth & Planet Sci.* **8**, 489–525.

Scholz, C. H. 1987. Wear and gouge formation in brittle faulting. *Geology* **15**, 493–495.

Scholz, C. H. 1990. *Mechanics of Faulting and Earthquakes*. Cambridge University Press, Cambridge.

Schwartz, D. P. & Coppersmith, K. J. 1984. Fault behavior and characteristic earthquakes: Examples from the Wasatch and San Andreas fault zones. *J. geophys. Res.* **89**, 5681–5698.

Sibson, R. H. 1986. Brecciation processes in fault zones: inferences from earthquake rupturing. *Pure & Appl. Geophys.* **124**, 159–175.

Sibson, R. H. 1988. Earthquake faulting as a structural process. *J. Struct. Geol.* **11**, 1–14.

Segall, P. & Pollard, D. D. 1980. Mechanics of discontinuous faults. *J. geophys. Res.* **85**, 4337–4380.

Segall, P. & Pollard, D. D. 1983. Nucleation and growth of strike-slip faults in granite. *J. geophys. Res.* **88**, 555–568.

Stein, R. S., King, G. C. P. & Rundle, J. B. 1989. The growth of geologic structures by repeated earthquakes, 2, Field examples of continental dip slip faults. *J. geophys. Res.* **93**, 13,319–31,331.

Tapponier, P. & Brace, W. F. 1976. Development of stress induced microcracks in Westerly granite. *Int. J. Rock Mech. & Mining Sci. Geomech. Abs.* **13**, 103–112.

Villemin, T., Angelier, J. & Sunwoo, C. In press. Fractal distribution of fault length and offset: Implications on brittle deformation evaluation: The Lorraine Coal Basin (NE France). In: *Fractals and Their Use in the Petroleum Industry* (edited by Barton, C. & LaPointe, P.). Am. Ass. Petrol. Geol. Book Series.

Wallace, R. E. & Morris, H. T. 1986. Characteristics of faults and shear zones in deep mines. *Pure & Appl. Geophys.* **124**, 107–125.

Watterson, J. 1986. Fault dimensions, displacements and growth. *Pure & Appl. Geophys.* **124**, 365–373.

Walsh, J. J. & Watterson, J. 1987. Distribution of cumulative displacement and of seismic slip on a single normal fault surface. *J. Struct. Geol.* **9**, 1039–1046.

Walsh, J. J. & Watterson, J. 1988. Analysis of the relationship between displacements and dimensions of faults. *J. Struct. Geol.* **10**, 239–247.

Walsh, J. J. & Watterson, J. 1989. Displacement gradients on fault surfaces. *J. Struct. Geol.* **11**, 307–316.

Walsh, J. J. & Watterson, J. 1991. Geometric and kinematic coherence and scale effects in normal fault systens. In: *The Geometry of Normal Faults. Spec. Publs. geol. Soc. Lond.* **56**, 193–206.